Chapter III
Experimental Work

A few compositions in the systems $Ce_{1-x-y}La_xSr_yO_{1.925}$, $Ce_{0.85}La_{0.15-x}Sr_xO_{\{2-(0.075+x/2)\}}$, $Ce_{1-x-y}Sm_xSr_yO_{1.90}$, $Ce_{1-x-y}Ca_xSr_yO_{2-\delta}$ and $Ce_{0.90}Mg_{0.10-x}Sr_xO_{1.90}$ were synthesized using citrate nitrate gel auto-combustion method. All the samples were characterized for their thermal behavior, crystal structure, microstructure, elemental analysis and electrical properties using DTA/TGA, X-ray diffraction, scanning electron microscope, energy dispersive spectroscopy and complex plane impedance analysis respectively. A list of raw materials used in the synthesis of these systems is given in Table. 2.1.

Table. 3.1 List of chemicals used

S. No.	Materials Used	Chemical Formula	Purity	Manufacturer
1.	Ammonium ceric nitrate	$(NH_4)_2[Ce(NO_3)_6]$	99.00%	Qualikems
2.	Lanthanum oxide	La_2O_3	99.90%	Sigma Aldrich
3.	Samarium oxide	Sm_2O_3	99.99%	Indian Rare Earth Ltd., India
4.	Strontium nitrate	$Sr(NO_3)_2$	99.50%	Reidel Chemicals
5.	Magnesium nitrate	$Mg(NO_3)_2$	99.50%	Qualigens
6.	Calcium carbonate	$CaCO_3$	99.50%	Reidel Chemicals
7.	Citric acid	$C_6H_8O_7$	99.50%	Loba chemie, India
8.	Lithium carbonate	Li_2CO_3	97.00%	Thomas baker Pvt. Ltd. chemicals, India
9.	Sodium carbonate	Na_2CO_3	99.90%	Thomas baker Pvt. Ltd. chemicals, India

3.1 Preparation of Materials

3.1.1 Preparation of nitrates

La_2O_3 and Sm_2O_3 were heated at 800 °C for 1 hr in a platinum crucible to remove the adsorbed moisture and then cooled in the furnace to 500 °C. Thereafter, these were transferred to a desiccator for cooling to room temperature. These were weighed quickly to avoid any adsorption of moisture again. $La(NO_3)_3$, $Sm(NO_3)_3$ and $Ca(NO_3)_2$ were prepared by dissolving required amount of La_2O_3, Sm_2O_3 and $CaCO_3$ in dilute nitric acid followed by heating at 100 ºC to complete dryness. This gives $La(NO_3)_3$, $Sm(NO_3)_3$ and $Ca(NO_3)_2$ which were then dissolved in distilled water to get an aqueous transparent solution. A flow chart for the preparation of nitrates is shown in Fig. 3.1.

3.1.2 Synthesis of ceria powders by citrate-nitrate gel auto-combustion method

All the doped or co-doped ceria powders were prepared using citrate nitrate gel auto-combustion route. Nanocrystalline powders can be easily synthesized by this processing route at low cost and in less time. Citrate nitrate auto-combustion route has many advantages over other methods e.g. solid state route, sol-gel route, chemical co-precipitation etc. This gives high purity product with very fine particles in the nanosize range and good chemical homogeneity. This method requires very simple equipments and cheap materials e.g. nitrate of metals. The source of energy for auto-combustion process is the exothermic decomposition of the redox mixture of metal nitrates with citric acid. In these mixes, metal nitrates and citric acid act as an oxidizer and the fuel respectively.

All the chemicals were accurately weighed in stoichiometric amounts. Ammonium ceric nitrate, metal nitrates and citric acid were separately dissolved in de-ionized water to make transparent aqueous solutions. Solutions of ammonium ceric nitrate and metal nitrates were mixed to the aqueous solution of citric acid to achieve a citrate to nitrate (C/N) molar ratio of 0.3 for controlled combustion [Basu et al. (2004)]. The mixed solutions were heated continuously at 200 ºC on a hot plate using a magnetic stirrer to evaporate excess water. After sometime, solution became

viscous, turned into a gel and auto-ignition occurred with evolution of large volume of the gases such as H_2O, NO_2 and CO_2. This leaves a yellow color porous ash in the container. The ash was calcined based on the results of DTA/TGA in a platinum crucible using an electrical furnace. Fig. 3.2 shows the flow chart for the preparation of ceria powders. The temperature and time of the calcination of all the compositions is given in Table. 3.2.

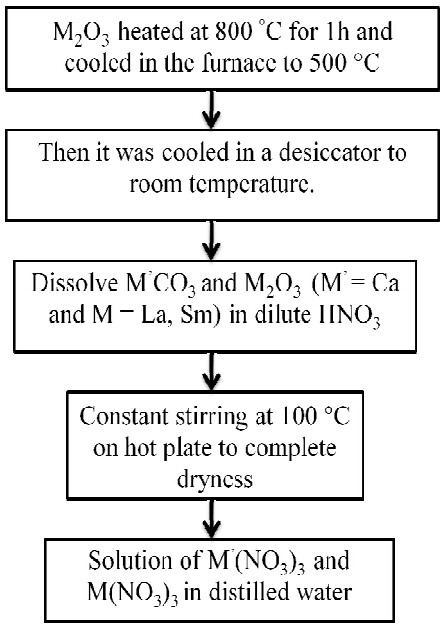

Fig. 3.1 Flow chart for preparation of nitrates

Table. 3.2 Calcination temperature and time of all the compositions

S. No.	Compositions	Temperature (°C)	Time (h)	Heating rate/cooling rate (°C/min)
1.	$Ce_{1-x-y}La_xSr_yO_{1.925}$	800	4	5/5
2.	$Ce_{0.85}La_{0.15-x}Sr_xO_{2-\delta}$	800	4	5/5
3.	$Ce_{1-x-y}Sm_xSr_yO_{1.90}$	800	4	5/5
4.	$Ce_{1-x-y}Ca_xSr_yO_{2-\delta}$	600	4	5/5
5.	$Ce_{0.90}Mg_{0.10-x}Sr_xO_{1.90}$	800	4	5/5

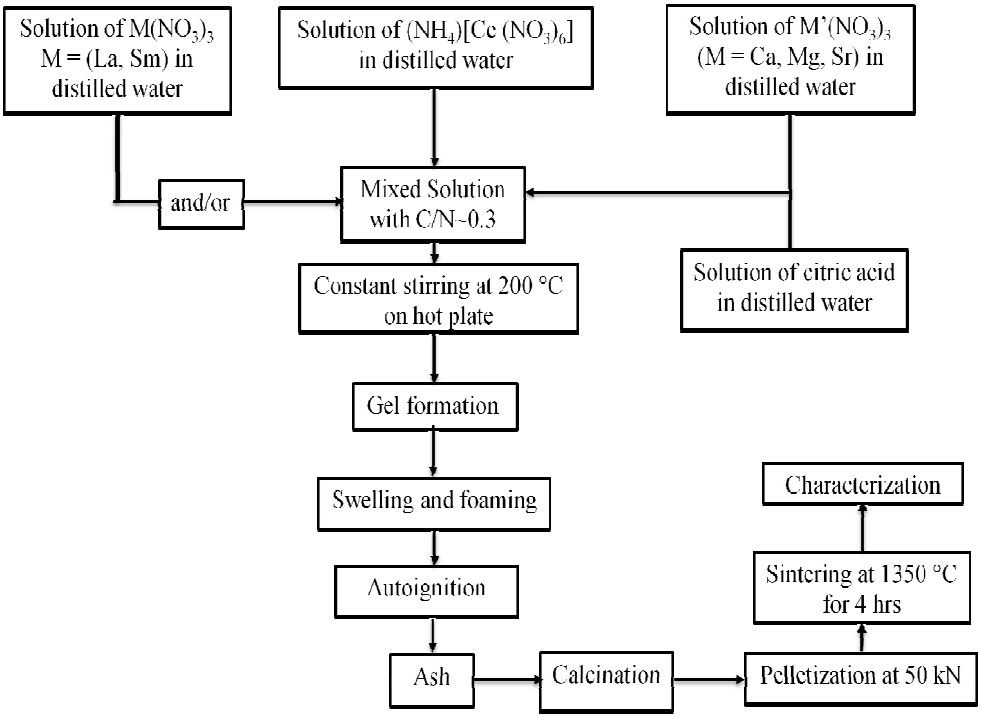

Fig. 3.2 Flow chart for synthesis of ceria powders

3.1.3 Preparation of nanocomposites

Nanocrystalline co-doped ceria powders prepared by citrate nitrate route were mixed with the eutectic binary mixture of Li_2CO_3 and Na_2CO_3 [$(Li_{0.52}Na_{0.48})_2CO_3$)] in different weight ratio of 80:20, 70:30 and 65:35. The carbonate content was not used above 35 wt% to prevent the de-shaping of the sample during sintering [Huang et al. (2007)]. The mixtures were milled for 5 h in acetone using Fritsch Pulverisette Ball Mill employing zirconia jars and zirconia balls as a grinding media. Milled powders were dried in an oven at 60 °C for 24 hrs. Dried powders were calcined at 600 ^{o}C (according to DTA results) for 2 hrs in air in a platinum crucible. A flow chart for the preparation of nanocomposites is shown in Fig. 3.3.

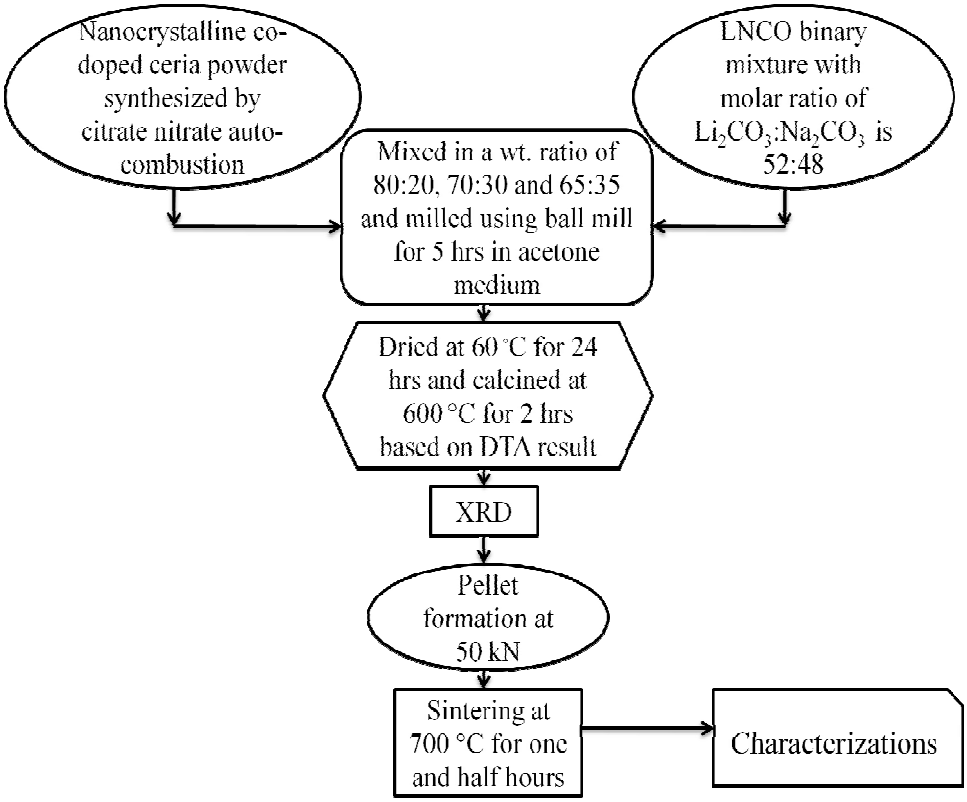

Fig. 3.3 Flow chart of the preparation of nanocomposites

3.2 Pellet formation and sintering

The calcined powders were pressed uniaxially using hydraulic press into cylindrical pellets (diameter~15 mm, thickness~2 mm) with an optimized load of 50 kN as shown in Fig. 3.4. Five pellets were made of equal weight at different loads. Density of each pellet was determined by measuring its dimension. A plot of green density vs. load was plotted as shown in Fig. 3.4 and fitted using a non linear fitting program. Pellets of all the ceria powders and nanocomposites were sintered at 1350 ºC for 4h and 700 ºC for $1\frac{1}{2}$ h respectively on a platinum foil at a heating and cooling rate of 5 ºC/min using a Lenton furnace made in Germany. The samples were furnace cooled to the room temperature at 5 ºC/min.

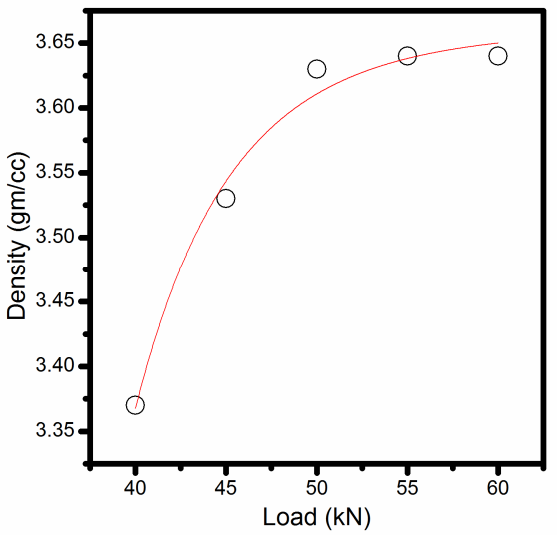

Fig. 3.4 Optimization of load

3.3 Characterizations

3.3.1 Thermal analysis

DTA/TGA is a technique used to study the changes in a sample on heating. TGA automatically records the change in weight of a sample as a function of temperature or time. Change in a weight, ΔW, is a fundamental property of the sample used for quantitative calculations of compositional changes. DTA measures the difference in temperature ΔT, between a test sample and an inert reference sample as a function of temperature. Temperature difference, ΔT remains zero until some thermal events occur e.g. decomposition, melting, phase transformation etc.

DTA/TGA of the as-prepared ash of ceria and milled composite powders was done using SETARAM and NETZSCH Gerate Bau TGA/DTA in the temperature range 30-1000 °C and 30-800 °C respectively in N_2 atmosphere at a heating rate of 10 °C/min. Fig. 3.5 shows an image of NETZSCH Gerate Bau DTA/TGA. A few milligrams of the test sample and an inert reference sample, Al_2O_3 powder were placed in two alumina crucibles and put side by side in a heating block. Identical thermocouples were placed in each crucible and connected back to back.

Fig. 3.5 NETZSCH Gerate Bau DTA/TGA

[www.netzsch-thermal-analysis.com]

The net e.m.f., therefore, represents the temperature difference between the test sample and reference sample. The two crucibles were heated at a constant rate and the temperature difference is plotted either against the time or temperature. Any thermal changes occurring in the test sample will cause its temperature to either lag behind or lead the temperature of reference sample corresponding to an endothermic and exothermic peak respectively.

3.3.2 Powder X-ray diffraction

X-ray diffraction is a non-destructive technique used to determine the phases and crystal structure of a material. X-ray diffractometer is basically designed as a Debye-Scherrer camera, except that the strip of film is replaced by a movable counter. Fig. 3.6 shows the schematic diagram of X-ray diffractometer. It consists of a source of monochromatic radiation and X-ray detector on the circumference of a circle. This circle is centered on the powder specimen and divergent slits, located specimen and detector. It limits the scattered radiation and reduces noise. Monochromatic radiations used in the X-ray are produced by copper target and a Ni filter whose characteristic

wave length for K_α-line is 1.54059 Å. The detector and specimen holder are mechanically coupled with a goniometer so that a rotation of the counter through 2θ degrees is automatically accompanied by rotation of the specimen through θ degree. This coupling ensures that the angle of incidence on and reflection from, the specimen will always be equal to one another and half of the angle of diffraction [Cullity (1959)]. Diffractometer measures the diffraction pattern depending on the kind of circuit used to measure the rate of producing pulses in the counter. The succession of pulses is converted into steady current which is measured on a meter called a counting meter, calibrated in such units as counts per second. This gives a continuous indication of X-ray intensity.

Powder X-ray diffraction patterns of the calcined and sintered powders were recorded using a Rigaku high resolution powder X-ray diffractometer employing Cu $K_{\alpha 1}$ radiation and Ni-filter at room temperature. Data were collected in the Bragg angle range of $20° \leq 2\theta \leq 80°$. Diffraction peaks were indexed using JCPDS standard files. Lattice parameter was determined using nonlinear least square fitting "Unit Cell" software [Holland T. et al. (1997)]. Average crystallite size, D was determined using Scherrer's formula:

$$D = \frac{0.9\lambda}{\beta cos\theta} \tag{3.1}$$

where β is the full width at half maxima (FWHM) excluding instrumental broadening, λ is the wave length of X-rays and θ is Bragg angle. β is taken for the strongest Bragg's peak corresponding to (111) reflection for all the samples.

$$\beta = \sqrt{\beta_m^2 - \beta_s^2} \tag{3.2}$$

where β_m and β_s are the FWHM of the powder and broadening of the peak corresponding to (111) reflection.

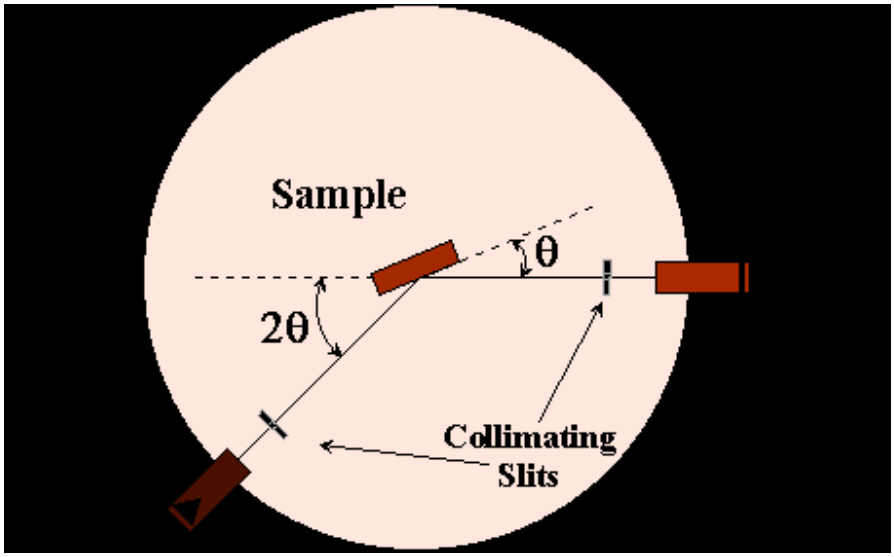

Fig. 3.6 Schematic diagram of X-ray diffractometer [http//www.wikipedia.com]

3.3.3 Density and porosity measurements

Density of sintered pellets was determined by Archimedes principle using the following formula:

$$Bulk\ Density = \frac{W_d}{W_s - W_a} \times Density\ of\ Kerosene \quad (3.3)$$

where, W_d, W_s and W_a are the dry weight, soaked weight and suspended weight of the sample respectively. Density of kerosene is 0.81 gm/cm^3. Theoretical density of doped ceria samples was calculated from the molecular wt. of the sample and lattice parameter using the following formula:

$$Theoretical\ density = \frac{Theoretical\ density - Experimental\ density}{Theoretical\ density} \times 100 \quad (3.4)$$

Theoretical density, ρ of the composites was calculated by the mixture rule using the following formula:

$$\rho = \rho_a V_a + \rho_b V_b \quad (3.5)$$

where, ρ_a, ρ_b, V_a and V_b are the density of ceria phase, carbonate phase, volume fraction of the ceria phase and carbonate phase respectively. Density of the binary carbonates mixture [$(Li_{0.52}Na_{0.48})_2CO_3$] was taken as 2.30 g/cm^3 [Zhao et al. (2013)]

3.3.4 Field emission scanning electron microscopy (FE-SEM) equipped with energy dispersive X-ray spectroscopy (EDS)

Scanning electron microscope (SEM) is an electron microscope which uses a beam of electrons instead of light to produce an image of a sample by scanning it. Electron beam is thermionically emitted from an electron gun fitted with a tungsten filament cathode. SEM has a large depth of focus due to very fine electron probe and producing very much magnified image more than 500,000 times. SEM uses a very fine probe of electrons with energies up to 30 or 40 keV passing through scanning coils focused at the surface of the specimen and scanned across it in a pattern of parallel lines. Once the beam hits the surface of the specimen, different types of signals are produced including; back scattered electrons, secondary electrons, characteristic X-rays. Intensity of emission of both the secondary and back scattered electrons depends on the angle at which the electron beam strikes the specimen surface. Detector collects these signals and converts them into a signal that is sent to a monitor screen which produces the final image.

In FE-SEM, a field emission cathode is placed in the electron gun which produces narrower probing beams with a high electron energy resulting in high resolution images i.e. 3 to 6 times better than the conventional SEM images. By using FE-SEM, a high quality and low voltage images can be produced with negligible sample charging. Fig. 3.7 shows the working principle of FE-SEM. As the electron beam is passed through the sample surface, it produces X-ray fluorescence from the atoms in its path. The energy of each X-ray photon is the characteristic of the element which produces it. Energy dispersive X-ray spectroscopy collects these X-rays and plots a spectrum which shows the number of X-rays collected at each energy.

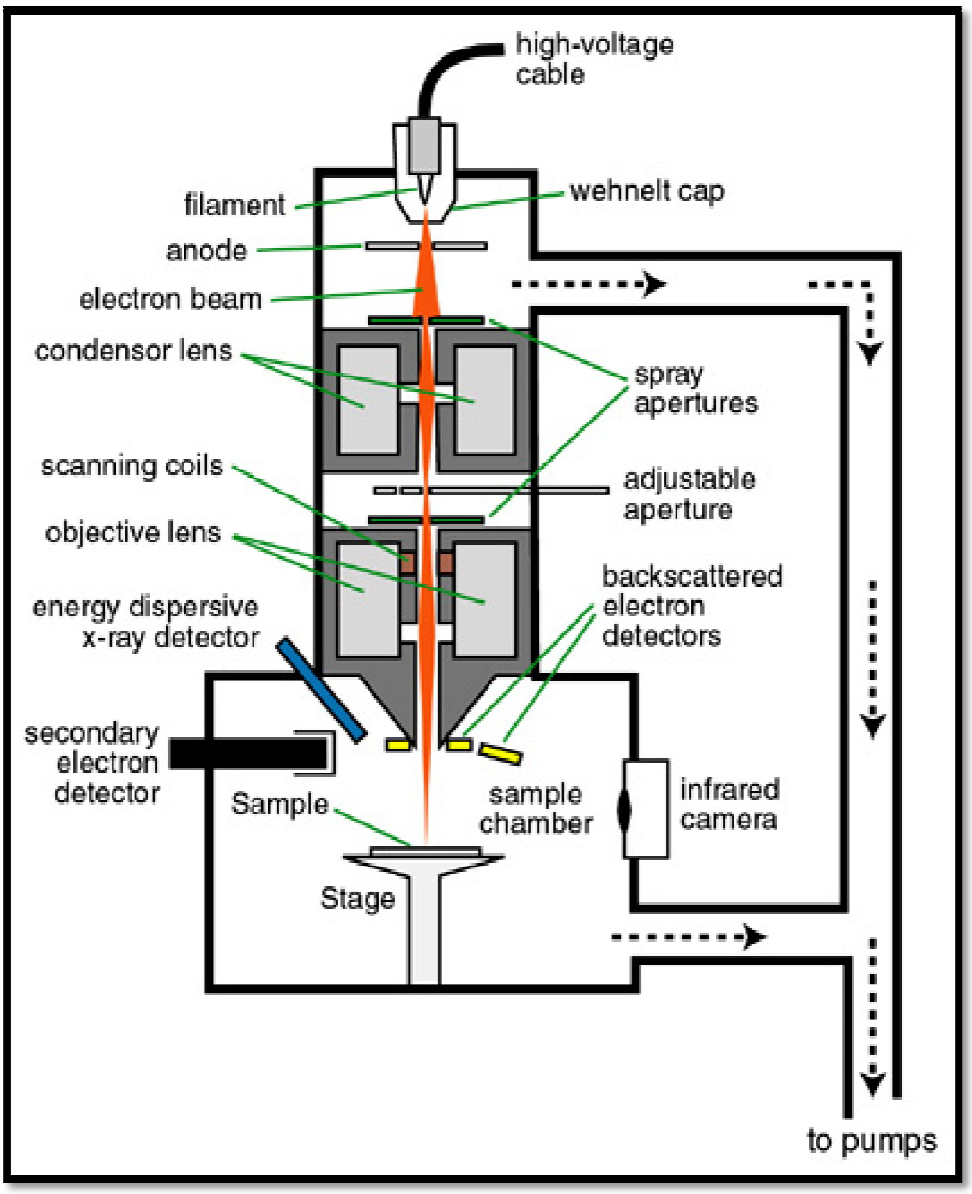

Fig. 3.7 Working principle of FE-SEM [http:/www4.nau.edu]

Fig. 3.8 Image of FEI NOVA NANOSEM (www.fei.com/products/sem/nova-nanosem)

Sintered pellets were polished using emery papers of grade 1/0, 2/0, 3/0, and 4/0 (Sia, Switzerland) followed by polishing on a velvet cloth using diamond paste of grade1/4-OS-475 (HIFIN). Then these were etched thermally at 1250 ℃ for 20 min at a heating and cooling rate of 10 ℃/min using a Lenton furnace. Composite samples were polished in the same manner and chemically etched with HCL (38 % concentration) for 20 sec. Micrographs and EDS spectrum of thermally and chemically etched samples were taken using a INSPECT 50 FEI scanning electron microscope, SUPRA 40 Zeiss and FEI NOVA NANOSEM field emission scanning electron microscope equipped with EDX. Fig. 3.8 shows an image of FEI NOVA NANOSEM.

3.3.5 Coefficient of thermal expansion (CTE) using dilatometer

A dilatometer measures the change in dimensions of a material when it is heated or cooled. A pushrod dilatometer (V. B. Ceramics, Chennai, India) was used to measure the CTE of composite samples. Fig. 3.9 shows an image of pushrod dilatometer.

Pushrod dilatometry, as its name implies, involves intermediary machine member to transmit the dimensional change caused in a sample by a change in the temperature. CTE was calculated using the following formula:

$$\alpha_{T_2-T_1} = \frac{dL}{L_0\,(T_2-T_1)} \tag{3.6}$$

where dL and L_0 are the change in the length and initial length of the sample respectively. T_2 and T_1 are the final and initial temperature respectively.

Fig. 3.9 Image of pushrod dilatometer [www.vbceramics.com]

For CTE measurements, rectangular bars of dimension 50 mm ×10 mm ×4 mm were prepared using a rectangular die made of stainless steel under a load of 50 kN. These bars were sintered at 700 °C for one and half an hour with a heating rate of 5 °C/min. The measurements were made in the range from room temperature to 700 °C with a heating rate of 10 °C/min in air atmosphere.

3.3.6 Complex plane impedance analysis

Polycrystalline ceramics when subjected to an alternating electric field show the contributions from the grains (bulk), grain boundaries and electrode/specimen polarizations to the total polarization. Complex plane impedance analysis is a powerful tool to separate these contributions. AC response of polycrystalline

electrolytes can be expressed by using the following formalisms [Hodge et al. (1976)]:

$$Z^* = Z' - iZ'' = R_s - {}^{j}/_{\omega C_s} = \frac{1}{Y^*} \quad (3.7)$$

$$Y^* = Y' + iY'' = \frac{1}{R_p} + j\omega C_p = i\omega c_0 \in^* \quad (3.8)$$

$$M^* = M' + jM'' = \frac{1}{\epsilon^*} \quad (3.9)$$

$$\epsilon^* = \epsilon' - i\,\epsilon'' \quad (3.10)$$

$$Tan\delta = \frac{\epsilon''}{\epsilon'} = \frac{M''}{M'} = \frac{Z'}{Z''} = \frac{Y'}{Y''} \quad (3.11)$$

where suffixes p and s represent the parallel and series elements of the circuit respectively. The terms Z^*, Y^*, M^*, ε^*, C_0 and ω are the complex impedance, admittance, modulus, permittivity, geometrical capacitance and frequency respectively. Plots of Z'' vs Z' and M'' vs M' are called Complex plane plots. Plots of Z'' and M'' vs log f are known as the Spectroscopic plots. In the complex plane impedance plot, relaxation frequencies of different polarization processes increases from left to right and vice versa in the complex plane modulus plots. The AC response of a polycrystalline material which has contributions from the grains, grain boundaries and electrode/specimen interface can be represented by an equivalent circuit shown in Fig. 3.10 [Hodge et al. (1976)]. The equivalent circuit contains three parallel resistance (R) and capacitance (C) circuits connected in series for the grains, grain boundaries and electrode/specimen polarizations respectively.

In Fig. 3.10 a constant phase element (CPE) was used in place of an ideal capacitor. This is due to presence of microstructural inhomogeneties in the materials. CPE is equivalent to the distribution of capacitors in the parallel. R_1, R_2, R_3, CPE1, CPE2 and CPE3 are the resistance and capacitance of the grains, grain boundaries and electrode respectively. The capacitance associated with the bulk, grain boundaries and electrode processes are in the range pF, nF and µF respectively determined from the relation $2\pi f_{max}RC = 1$, where f_{max} is the frequency at the arc maximum and R is the resistance determined from the intercept on the real Z' axis as shown in Fig. 3.10.

Three depressed circular arcs are observed in the impedance plot in the high, intermediate and low frequency range corresponding to contribution of the grains, grain boundaries and electrode/specimen interface to the total resistance respectively. Circular arcs are obtained when each of the contribution has single value of relaxation time. In case there is a distribution of relaxation times for a particular contribution, then a depressed circular arc is obtained for that contribution. One, two or three arcs are observed depending on the nature of the samples i.e. the sample is either a conductor or a semiconductor or an insulator. When all the three polarization processes have widely separated time constants, then three distinct semicircles are obtained and when they have time constant close to each other overlapping of arcs are obtained [Rajesh et al. (1999)]. Whether a full, partial or no semicircles are observed depends on the strength of the relaxation and experimental conditions. Strength of relaxation is defined as $\epsilon_s / \epsilon_\infty$ where ε_s is the static dielectric constant as $\omega \rightarrow 0$ and ϵ_∞ is the dielectric constant when $\omega \rightarrow \infty$.

For impedance measurements, both the surfaces of sintered pellets were polished using emery papers of grade 1/0, 2/0, 3/0, and 4/0 (Sia, Switzerland). Silver paste was coated on both the polished surfaces followed by drying at 100 ^{o}C in an electrical oven for 15 min. The paint was matured by heating at 700 ^{o}C for 15 min in an electrical furnace to make smooth conducting surfaces. Impedance measurements were made in the frequency range 1 Hz to 1 MHz in the temperature range 200–700 ^{o}C at an interval of 25 ^{o}C using a Novocontrol Alpha-A High Performance Frequency Analyzer. The accuracy of impedance data is in between ±0.2% to ±6%. The accuracy of the impedance data was determined from the manual of Novocontrol Impedance Analyzer and is also shown in the impedance plots for all the samples.

For comparison of the conductivity of the nanocomposites, impedance measurement of the molten binary carbonate mixture was also made in the same manner. There is about ±10 to ±12% error in the measurement due to disturbance of the molten carbonate phase.

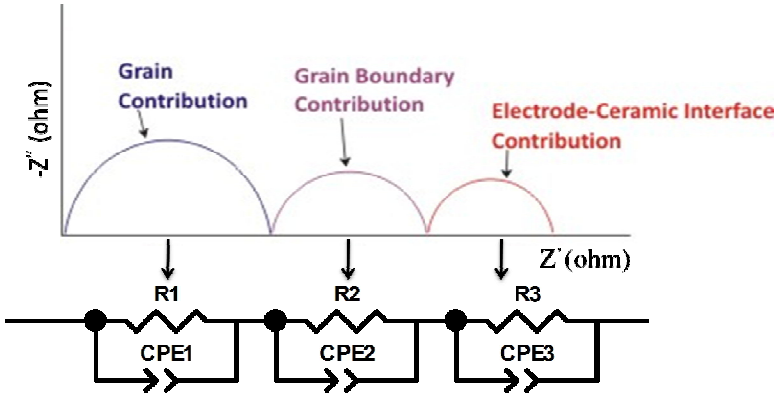

Fig. 3.10 A schematic representation of impedance plot of a polycrystalline solid electrolyte with an equivalent circuit

The silver coated pellets were placed in a sample holder as shown in Fig. 3.11. In this, a spring loaded electrode is fixed in a stainless steel plate which is insulated by Teflon circular cylinder and presses the pellet from the top. A lower plate which is situated below the sample surface serves as another electrode. These electrodes were connected to Alpha A High Performance Frequency Analyzer using a shielded co-axial cables. The whole sample cell assembly was placed inside a tube furnace. A temperature controller was connected to the furnace to control the rate of heating. The complex plane impedance plots were recorded on a monitor screen and data were collected using 'Win data' software. These data were fitted using 'ZView' software to distinguish the contribution of the grains and grain boundaries to the total resistance.

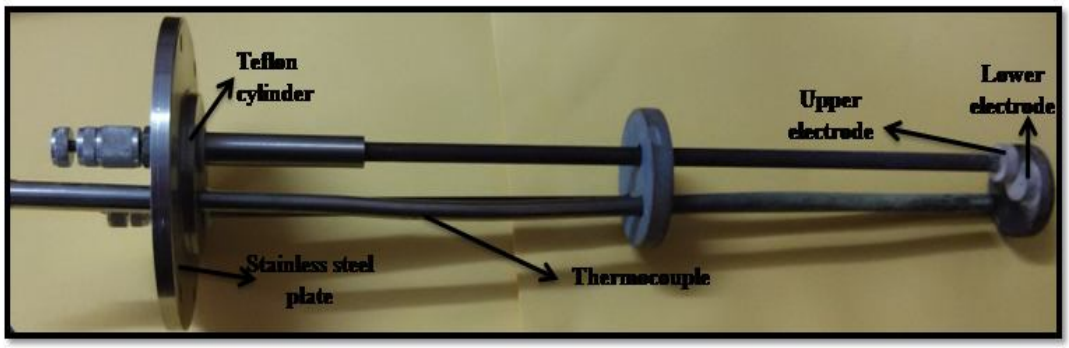

Fig. 3.11 A schematic diagram of sample cell used in impedance measurements

Then, conductivity of the grains and the grain boundaries were determined and fitted to Arrhenius equation. Plots of Log σT vs. 1000/T were fitted using linear fitting program to calculate the activation energy of conduction and the pre-exponential factor. Conductivity of the grains, σ_g was calculated using the formula:

$$\sigma_g = \frac{L}{S \times R_1} \tag{3.12}$$

where, L, S and R_1 are the thickness, surface area and resistance of the grains of the sample respectively. Conductivity of the grain boundaries, σ_{gb}^*, was determined using the formula:

$$\sigma_{gb}^* = \frac{L}{S \times R_2} \times \frac{CPE1}{CPE2} \tag{3.13}$$

where, R_2, CPE1 and CPE2 are the resistance of the grain boundaries, capacitance of the grains and grain boundaries respectively. σ_{gb}^* is the specific grain boundaries conductivity which will be discussed in detail in the next chapter. Total conductivity, σ_t, was determined using the formula:

$$\sigma_t = \frac{L}{S \times (R_1 + R_2)} \tag{3.14}$$

where R_1+R_2 is the total resistance R_t of the electrolyte.